Coarse-grained modeling of the structural states and transition underlying the powerstroke of dynein motor domain

Wenjun Zheng

Citation: J. Chem. Phys. **136**, 155103 (2012); doi: 10.1063/1.4704661
View online: http://dx.doi.org/10.1063/1.4704661
View Table of Contents: http://jcp.aip.org/resource/1/JCPSA6/v136/i15
Published by the American Institute of Physics.

Coarse-grained modeling of the structural states and transition underlying the powerstroke of dynein motor domain

Wenjun Zheng[a)]
Physics Department, University at Buffalo, Buffalo, New York 14260, USA

(Received 1 February 2012; accepted 3 April 2012; published online 19 April 2012)

This study aims to model a minimal dynein motor domain capable of motor function, which consists of the linker domain, six AAA+ modules (AAA1–AAA6), coiled coil stalk, and C-terminus domain. To this end, we have used the newly solved X-ray structures of dynein motor domain to perform a coarse-grained modeling of dynein's post- and pre-powerstroke conformation and the conformational transition between them. First, we have used normal mode analysis to identify a single normal mode that captures the coupled motions of AAA1–AAA2 closing and linker domain rotation, which enables the ATP-driven recovery stroke of dynein. Second, based on the post-powerstroke conformation solved crystallographically, we have modeled dynein's pre-powerstroke conformation by computationally inducing AAA1–AAA2 closing and sliding of coiled coil stalk, and the resulting model features a linker domain near the pre-powerstroke position and a slightly tilted stalk. Third, we have modeled the conformational transition from pre- to post-powerstroke conformation, which predicts a clear sequence of structural events that couple microtubule binding, powerstroke and product release, and supports a signaling path from stalk to AAA1 via AAA3 and AAA4. Finally, we have found that a closed AAA3–AAA4 interface (compatible with nucleotide binding) is essential to the mechanochemical coupling in dynein. Our modeling not only offers unprecedented structural insights to the motor function of dynein as described by past single-molecule, fluorescence resonance energy transfer, and electron microscopy studies, but also provides new predictions for future experiments to test.
 [http://dx.doi.org/10.1063/1.4704661]

INTRODUCTION

Dyneins are giant cytoskeletal motors of 1–2 MDa that can utilize energy from ATP hydrolysis to move processively[1,2] toward the minus ends of microtubules (MT).[3] They are critically involved in a variety of functions in eukaryotic cells, including the beating of cilia and flagella, cell division, cell migration, and the intracellular trafficking of various vesicles and organelles along MT.[4–7]

The primary kinetic cycle of dynein, which is highly similar to another superfamily of cytoskeletal motors – myosin,[8] has been characterized by past studies:[8–12]

D-ATP → **D-ADP-Pi** → **M-D-ADP** → **M-D** → **D-ATP**

(**D**: dynein, **M**: MT, **Pi**: inorganic phosphate).

Starting from the **D-ATP** state, dynein is detached from MT and undergoes an isomerization,[10] which is accompanied by a rotation of the tail domain to the pre-powerstroke position (recovery stroke). Then, ATP hydrolysis leads to **D-ADP-Pi** state (pre-powerstroke state). MT binding and Pi release lead to **M-D-ADP** state (or two ADP states linked by an isomerization, see Refs. 10–12), resulting in force generation (powerstroke) as the tail domain rotates to the post-powerstroke position. Subsequent release of ADP leads to **M-D** state. ATP binding dissociates dynein rapidly from MT, and returns it to **D-ATP** state for the next cycle. During the above kinetic cycle, ADP release is rate limiting[12] and accelerated by MT binding.[11,13]

The structural architecture of dynein has been well characterized. The heavy chain of dynein consists of a tail, a head, and a stalk. The tail is responsible for dimerization of the heavy chain and binding of associated proteins and cargo,[14,15] but it is dispensable for dynein's processive motility.[2] The N-terminus region of the head (∼10 nm long, named the linker domain) is thought to be critically involved in the powerstroke of dynein motor.[10,16–18] The rest of the head consists of six tandemly linked AAA+ modules (AAA1–AAA6) (Refs. 19 and 20) and C-terminus domain forming a ring with a diameter of ∼13 nm (Ref. 21) (see Fig. 1). Each module is a member of the AAA+ (ATPase associated with diverse cellular activities) superfamily of mechanochemical enzymes.[22] The hexameric ring is solely responsible for dynein's core motor activities, such as ATP hydrolysis, ATP-dependent MT binding, and MT-based motility.[23,24] Among the four AAA+ modules (AAA1–AAA4) that can bind ADP and/or ATP,[25] AAA1 has the primary ATPase site,[9] AAA3 has a secondary ATPase site[26] which was shown to play an important role in dynein motility,[27–29] while AAA2 and AAA4 can bind nucleotide and play certain regulatory role.[30,31] A 12-nm-long coiled coil stalk ends in a globular MT-binding domain (MTBD) that binds MT in an ATP-dependent manner.[23]

The molecular mechanism of dynein motility remains poorly understood, which is mainly due to the lack of high-resolution dynein structures until recently. In the past, low-resolution structural information of dynein from electron

[a)]Electronic mail: wjzheng@buffalo.edu.

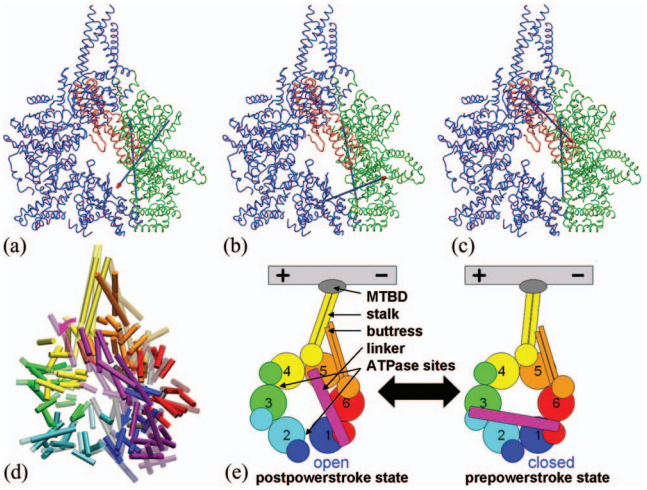

FIG. 1. Results of NMA and structural alignment for dynein motor domain: Panels (a)–(c) show the dynamic domain partition for modes 1–3, respectively; domains 1–3 are colored red, green, and blue, respectively; the axis of the rotation of domain 1 (2) relative to domain 3 is represented by an arrow with blue stem and red (green) tip. Panel (d) shows the structural alignment in helices between two X-ray structures of dynein motor domain (PDB codes: 3qmz and 3ay1, shown as opaque and transparent, respectively); AAA1–AAA6 are colored blue, cyan, green, yellow, orange, and red; linker domain is colored purple; two arrows show the rotation of linker and further closing of AAA1–AAA2 interface from 3qmz to 3ay1. Panel (e) shows a cartoon for both pre- and post-powerstroke conformations of dynein motor domain; the large/small domain of each AAA+ module is represented by a large/small circle; key parts of dynein are labeled; the same color scheme as panel (d) is used for AAA1–AAA6 and linker; also shown are the MTBD (colored gray) and MT (colored light gray, with plus and minus ends marked).

microscopy (EM) has shed lights on the structural basis of dynein motility. In an early EM study, it was found that the tail is in two different positions when dynein is at nucleotide-free and ADP-vanadate(Vi)-bound state.[16] The existence of two tail conformations during the kinetic cycle of dynein was confirmed by a fluorescence resonance energy transfer (FRET) study.[10] Therefore, a large rotation of tail may be involved in the powerstroke that drives the robust MT sliding observed by an *in vitro* motility assay study.[32] Furthermore, the tail rotation was shown to be coordinated with the cyclic MT association/dissociation at most intermediate states of the dynein kinetic cycle.[9]

Recently, two X-ray structures of dynein motor domain have been solved – one from *Dictyostelium discoideum* in the presence of ADP,[33] and another from yeast in the absence of nucleotide,[34] which offered a detailed view to the structural architecture of the functional units required for dynein's motor activity. However, both structures correspond to the post-powerstroke state of dynein while the pre-powerstroke conformation remains unknown. The objective of this study is to computationally model the pre-powerstroke conformation and the transition from pre- to post-powerstroke conformation.

Structure-based computer modeling has been increasingly employed to complement experimental efforts to elucidate the structural basis of various molecular motors. Nevertheless, the very long time scale of the kinetic cycle of many molecular motors has hampered extensive molecular dynamics (MD) simulations of conformational changes between different biochemical states. Additionally, the large size of dynein and relatively low resolution of the new X-ray structures pose great challenge to all-atom MD simulations of dynein.

To overcome the time-scale barrier, coarse-grained modeling has been developed using simplified structural representations and energy functions.[35] A good example of coarse-grained models is the elastic network model (ENM) which represents a protein structure as a network of C_α atoms connected by springs.[36–38] In an ENM, the all-atom force fields are replaced by harmonic potentials with a uniform force constant.[39] The normal mode analysis (NMA) of ENM yields low-frequency modes which were found to compare well with many crystallographically observed structural changes.[37,40] Numerous studies have established ENM as an effective means to model protein conformational dynamics based on low-resolution structures with virtually no limit in time scale or system size (for reviews, see Refs. 41 and 42). Recently, ENM has been employed to study the conformational dynamics of two cytoskeleton motors – myosin[43–55] and kinesin.[43,44,48,52] These studies have demonstrated the usefulness of coarse-grained modeling in probing the conformational dynamics of molecular motors.

Prior to the availability of dynein X-ray structures, Dokholyan and co-workers constructed a homology model of dynein, and then performed NMA, MD simulation, and kinetic modeling.[56–58] In this study, by using the new X-ray structures of dynein, we have performed a coarse-grained modeling of dynein's post- and pre-powerstroke conformation and the transition between them. First, we have used NMA to identify a single normal mode that captures the coupled motions of AAA1–AAA2 closing and linker domain rotation in support of the ATP-driven recovery stroke. Second, we have constructed a new structural model for dynein's pre-powerstroke conformation by computationally inducing AAA1–AAA2 closing and sliding of coiled coil stalk. Third, we have modeled the conformational transition from pre- to post-powerstroke conformation, which outlines a clear sequence of structural events in support of the allosteric couplings between MT binding, powerstroke, and product release. Finally, we have found that a closed AAA3–AAA4 interface is essential to the mechano-chemical coupling in dynein. Our modeling results offer structural insights to past experimental studies and provide new predictions for future experiments.

METHODS

Elastic network model and normal mode analysis

In an ENM, a protein structure is represented as a network of beads each corresponding to the C_α atom of an amino acid residue. A harmonic potential accounts for the elastic interaction between a pair of C_α atoms that are within a cutoff distance R_c chosen to be 10 Å (following Ref. 59). The ENM potential energy is

$$E = \frac{1}{2}\sum_{i=1}^{N}\sum_{j=1}^{i-1} k_{ij}\theta\left(R_c - d_{ij}^0\right)\left(d_{ij} - d_{ij}^0\right)^2, \qquad (1)$$

where N is the number of C_α atoms, $\theta(x)$ is the Heaviside function, d_{ij} is the distance between the C_α atom i and j, and d_{ij}^0 is the value of d_{ij} as given by an equilibrium structure (usually a crystal structure). k_{ij} is the force constant, which is 1 for non-bonded interactions and 10 for bonded interactions between residues (the unit of k_{ij} can be arbitrarily chosen without changing the modeling results). The use of high/low force constant for bonded/non-bonded pairs of C_α atoms was previously found to improve the accuracy of ENM-based modeling.[60]

We can expand the ENM potential energy to second order

$$E \approx \frac{1}{2} X^T H X, \tag{2}$$

where X is a $3N$-dimension vector representing the 3D displacement of N C_α atoms away from their equilibrium positions, H is the Hessian matrix which is obtained by calculating the second derivatives of ENM potential energy with respect to the 3D coordinates of C_α atoms.

Normal mode analysis solves $H W_m = \lambda_m W_m$, where λ_m and W_m represent the eigenvalue and eigenvector of mode m. After excluding 6 zero modes corresponding to 3 rotations and 3 translations, we keep $3N$-6 non-zero modes, which are numbered from 1 to $3N$-6 in order of ascending eigenvalue.

To validate ENM-based NMA, we compare each mode (mode m) with the observed structural changes between two crystal structures (represented by a $3N$-dimension vector X_{obs}) by calculating the following overlap:

$$I_m = \frac{\left| X_{obs}^T W_m \right|}{|X_{obs}| \cdot |W_m|}, \tag{3}$$

where $X_{obs}^T W_m$ is the dot product between X_{obs} and W_m, $|X_{obs}|$ and $|W_m|$ represent their magnitudes.

In addition, the following cumulative overlap is calculated to assess how well the lowest M modes describe X_{obs}

$$C_M = \sqrt{\sum_{1 \le m \le M} I_m^2}. \tag{4}$$

Because $\sum_{1 \le m \le 3N-6} I_m^2 = 1$, C_M^2 gives the percentage of the observed structural changes captured by the lowest M modes.

Coarse-grained transition pathway modeling by iENM

In a recent study,[54] we proposed a general algorithm to generate a transition pathway (i.e., a series of intermediate conformations) between two given protein conformations (named beginning and end conformations). We first construct two single-well potentials (E_1 and E_2) whose minima are located at the two given conformations, respectively. Then, we construct a double-well potential $F(E_1, E_2)$ with two minima located at the two given conformations. Then, we solve the saddle point (SP) of $F(E_1, E_2)$ as follows:

$$0 = \nabla F(E_1, E_2) = \frac{\partial F}{\partial E_1} \nabla E_1 + \frac{\partial F}{\partial E_2} \nabla E_2, \tag{5}$$

which is equivalent to solving the following equation (after setting $\lambda = \frac{\partial F}{\partial E_1} / (\frac{\partial F}{\partial E_1} + \frac{\partial F}{\partial E_2})$):

$$0 = \lambda \nabla E_1 + (1 - \lambda) \nabla E_2, \tag{6}$$

where λ is a parameter of interpolation – as λ varies from 1 to 0, the saddle point traces a pathway that connects the beginning and end conformation. Because this pathway passes all possible SPs, it is independent of the mathematic form of $F(E_1, E_2)$.

Based on the above general formulation, we have developed an interpolated ENM (iENM) protocol[54] which solves the saddle points of a double-well potential $F(E_{ENM1} + E_{col}, E_{ENM2} + E_{col})$, where E_{ENM1} and E_{ENM2} are two ENM potentials (see Eq. (1)) based at the beginning and end conformations, and E_{col} is a steric collision energy.[54] Here, we will use iENM to generate a pathway from the pre- to post-powerstroke conformation of dynein.

The iENM can not only predict a pathway between two given global conformations, but also model an unknown global conformation (at end state) from a known global conformation (at beginning state) together with a given "target" local structure (at end state). The idea is to computationally induce the local structural change toward the given target structure and let the rest of protein to relax to a minimal-energy conformation. We have recently used this method to construct a complete structural model for myosin motor domain from an incomplete crystal structure.[61] For implementation, we construct a single-well potential E_1 based on the known global conformation at beginning state and E_2 based on the "target" local structure at end state. Then, we solve the saddle point equation (see Eq. (6)) with λ varying from 1 to 0, which generates a pathway whose last frame gives a global structural model for the unknown end state. Here, we will use iENM to generate the pre-powerstroke conformation of dynein.

Quantification of motional order of key protein parts during a transition

Following Ref. 62, a fractional progress parameter $f_{progress}$($f_{progress} \in [0, 1]$) is defined for an intermediate conformation along a transition pathway: $f_{progress} = l/L$, where l is the length of the part of the pathway from the beginning conformation to the intermediate conformation, while L is the total length of the pathway from the beginning conformation to the end conformation. The length of a pathway is computed approximately by summing up RMSDs between consecutive conformations along the pathway (separated by 0.1 Å in RMSD).

We use the predicted pathway to determine the motional order of several protein parts. To this end, the following reaction coordinate is defined for a given part S,[51]

$$RC_S = 0.5 \left(1 + \frac{RMSD_{S,1}^2 - RMSD_{S,2}^2}{RMSD_{S,obs}^2} \right), \tag{7}$$

where $RMSD_{S,1}$($RMSD_{S,2}$) is the RMSD of C_α atoms of part S between a given intermediate conformation and the beginning (end) conformation, and $RMSD_{S,obs}$ is the corresponding RMSD between the beginning and end conformations. RC_S varies from 0 to 1 as the transition proceeds from the beginning to the end conformation. For two protein parts S and S′, if $RC_S < RC_{S'}$ along the pathway (namely, $RC_{S'}$ ascends from

0 to 1 faster than RC_S), we can infer that the motion of S′ precedes that of S.

Structural alignment

To obtain the conformational change between two X-ray structures of dynein (PDB codes 3ay1 and 3qmz), we structurally align them using the Dali server (ekhidna.biocenter.helsinki.fi/dali_lite/). No sequence information is used during the alignment because the amino acid residue names of 3ay1 are unassigned. The alignment result is shown in Table S1 of the supplementary material.[76]

We also use Dali to structurally align different AAA modules within the yeast dynein structure (PDB code: 3qmz). In particular, we align AAA1–AAA2 with AAA3–AAA4 to model the open-to-close conformational change between them. The alignment result is shown in Table S2 of the supplementary material.[76] Of the six AAA+ modules, AAA1 and AAA3 are structurally most similar.[34]

RESULTS

We aim to model a minimal dynein motor domain capable of motor function, which comprises the N-terminus linker domain (shown to be necessary for dynein motility in Ref. 2), six AAA+ modules (AAA1–AAA6), coiled coil stalk, and C-terminus domain. Our modeling is based on two recently solved X-ray structures of dynein motor domain (PDB codes: 3qmz and 3ay1). We mainly use the former structure (PDB code: 3qmz) to perform NMA, model pre-powerstroke conformation, and simulate the transition from pre- to post-powerstroke conformation; the latter (PDB code: 3ay1) is only used to extract crystallographically observed conformational changes in dynein.

NMA of dynein structure predicts key functional motions

To deduce collective motions encoded in the X-ray structure of yeast dynein (PDB code: 3qmz), we have constructed a C_α-only ENM from the X-ray structure (without adding missing residues or optimizing atomic coordinates). Then, we have performed NMA based on the ENM potential (see Methods section). The yeast dynein structure is chosen over the other one (PDB code: 3ay1) for NMA because the latter has more missing residues (all β-strand residues are absent), which result in an insufficiently connected ENM and therefore many zero modes.

We have visually examined the collective motions captured by the lowest three modes (see Figs. 1(a)–1(c)). Mode 2 is of most interest. Dynamic domain partition[63] suggests that the collective motion of mode 2 can be described in terms of rigid-body rotations among the following three dynamic domains (see Fig. 1(b)):

1. Domain 1 consists of subdomains 1 and 2 of the linker domain (hinged at the subdomains 2–3 interface, see Fig. 4 in Ref. 34);
2. Domain 2 consists of subdomains 3 and 4 of the linker domain, the large domain of AAA1, the small domain of AAA5 (excluding buttress), AAA6, and C-terminus domain;
3. Domain 3 consists of the rest of the hexameric AAA+ ring (including stalk and buttress).

The rotation of domain 1 relative to domain 3 (around an axis roughly perpendicular to the hexameric ring plane, see Fig. 1(b)) captures the swing of linker domain underlying the powerstroke and recovery stroke of dynein.[16,34] The rotation of domain 2 relative to domain 3 (around an axis lying within the hexameric ring plane, see Fig. 1(b)) captures the following two functional motions: first, the closing of AAA1–AAA2 gap, which may couple to ATP binding and isomerization[10] at the primary ATPase site;[34] second, the tilting of stalk/buttress relative to the small domain of AAA5, which may couple to further structural changes (such as sliding, see below) in stalk leading to changing MT-binding affinity of MTBD.[33,34] We note that the sliding motion within the coiled coil stalk is not predicted by NMA, because it is energetically unfavorable in ENM.

Similar partition of dynamic domains is obtained for modes 1 and 3, although the directions of inter-domain rotations are different (see Figs. 1(a) and 1(c)). In mode 1, the rotation of domain 1 relative to domain 3 is around an axis roughly parallel to the hexameric ring plane (see Fig. 1(a)); in mode 3, the rotation of domain 1 relative to domain 3 is around an axis roughly parallel to the linker domain (see Fig. 1(c)). A similar rotation of domain 2 relative to domain 3 is found for all three modes (see Figs. 1(a)–1(c)).

To assess the relevance of lowest modes (particularly mode 2) to real conformational changes in dynein, we explore how well they can account for the observed differences between the two dynein X-ray structures (PDB codes: 3qmz and 3ay1). We structurally align the two X-ray structures using Dali (see Methods section). Although both X-ray structures (solved in the absence of nucleotide and in the presence of MgADP, respectively) correspond to the post-powerstroke state, they do exhibit significant differences (see Fig. 1(d)): the AAA1–AAA2 gap is more open in 3qmz, and the linker domain of 3qmz (3ay1) mainly contacts with AAA5 (AAA4) – resulting in a small counterclockwise rotation of linker from 3qmz to 3ay1. The above differences could represent conformational changes associated with ADP release.[33] Then, we compare each mode with the observed structural changes from 3qmz to 3ay1. Encouragingly, the lowest ten modes (out of total 6408 modes) capture >50% of the observed changes, and mode 2 has the highest overlap (∼0.45). Indeed, mode 2 nicely captures the observed structural differences in AAA1–AAA2 and linker domain (see Fig. 1(b)). Unlike mode 2, mode 1 (with overlap ∼0.23) does not compare well with the observed structural changes because it describes a different rotation of linker perpendicular to the hexameric ring plane, although such rotation may account for the detachment of linker from the dynein ring which may enable the dynein dimer to separate its two heads further apart to achieve large step sizes. In sum, ENM-based NMA gives a good description of conformational changes in dynein motor domain.

Modeling of pre-powerstroke conformation with closed AAA1–AAA2 gap and shifted registry of coiled coil stalk

Next, we will start from the post-powerstroke dynein structure (PDB code: 3qmz) and construct a coarse-grained structural model for the pre-powerstroke state. Our modeling considers two key properties of pre-powerstroke state – the closed primary ATPase site and the weak MT-binding affinity.

At the pre-powerstroke state, dynein is bound with ADP-Pi or ATP at the primary ATPase site between AAA1 and AAA2. In the X-ray structure of yeast dynein, there is a large gap between the large domains of AAA1 and AAA2,[34] suggesting no nucleotide binds to the primary ATPase site. However, the AAA3–AAA4 interface is in a closed conformation, which is compatible with the binding of nucleotide. Therefore, we postulate that the pre-powerstroke state requires the open-to-closed conformational change of AAA1–AAA2 interface. Then, we ask whether and how the AAA1–AAA2 closing triggers global conformational changes involving the linker domain and other AAA+ modules. To answer this question, we have employed the iENM protocol (see Methods section) to computationally induce the AAA1–AAA2 closing (toward the AAA3–AAA4 conformation of 3qmz) and let the rest of dynein to relax to a minimal-energy conformation. To enable unhindered motion of linker domain, we turn off the contact interactions between the linker and AAA5.

In addition to the closing of AAA1–AAA2 gap (and AAA5–AAA6 gap), our modeling predicts a ∼42° counterclockwise rotation of linker domain with its N-terminus end (residue 1364) moving by ∼6 nm (see Fig. 2(a)), which is close to the 8 nm step size of dynein.[2] This large rotation takes the linker domain from the post-powerstroke position (in contact with AAA5) to near the pre-powerstroke position (in contact with AAA2/AAA3[18]), although the actual pre-powerstroke position may require a larger swing of linker domain as shown in a recent EM study.[18] Two possible causes for the larger swing of linker (observed in EM) are as follows: 1. Our modeling largely preserves the linker–AAA1 contacts formed in the post-powerstroke X-ray structure, whose breaking may allow further swing of the linker in the counterclockwise direction. 2. Our modeling does not fully consider the flexibility of linker, which may enable additional displacement of the linker tip (for example, via hinge motions between subdomains of linker).

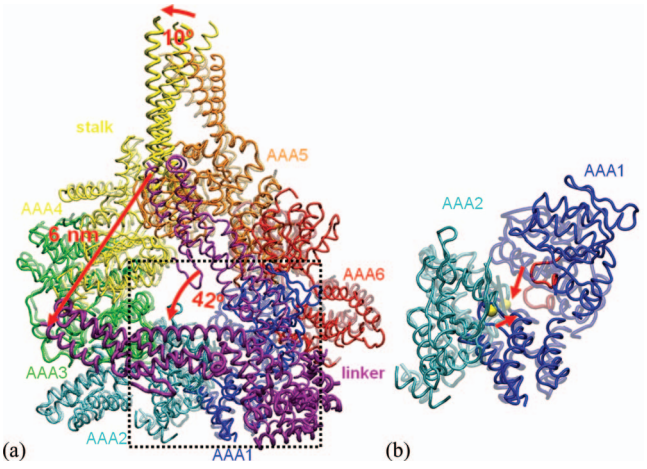

FIG. 2. Structural modeling of pre-powerstroke conformation of dynein motor domain: Panel (a) shows the model of pre-powerstroke conformation aligned with the post-powerstroke conformation (PDB code: 3qmz); the post-powerstroke conformation is opaque, while the pre-powerstroke conformation is transparent (except for the linker and stalk which are shown as thick opaque tubes); three red arrows show stalk tilting, linker rotation, and displacement of linker tip. Panel (b) shows an enlarged view of AAA1–AAA2 interface, where the Arginine finger of AAA2 is shown as a yellow bead and the Walker A motif of AAA1 is colored red. The same color scheme as Fig. 1(d) is used for AAA1–AAA6 and linker.

The directionality of the above structural changes (AAA1–AAA2 closing and linker domain rotation) has already been predicted by NMA (see Fig. 1(b)). Here, the iENM-based modeling further determines the magnitude of the above structural changes and yields a new structural model for the pre-powerstroke state without residue collision or bond distortion.

The finding that AAA1–AAA2 closing can directly trigger linker rotation suggests a strong coupling between the closing of primary ATPase site and the recovery stroke of dynein. This mechano-chemical coupling allows ATP binding and isomerization to detach the linker from its contact with AAA5,[34] and drive it to swing to the pre-powerstroke position, which may facilitate a fast transition from post- to pre-powerstroke state in the presence of ATP and absence of MT.[13] A similar mechano-chemical coupling mechanism works in F1 ATPase, where ATP binding is thought to induce an open-to-close hinge-bending motion of β subunit that pushes the γ stalk to rotate.[64] However, in myosin the closing of active site cannot directly induce the rotation of lever arm (functionally equivalent to dynein's linker domain). Instead, additional conformational changes (such as the bending of relay helix, see Ref. 65) or alternative mechanisms (such as thermally driven Brownian motion, see Ref. 66) are needed.

Another key property of pre-powerstroke state is its weak MT-binding affinity. As shown previously, a change in the registry of the coiled coil stalk allosterically couples ATP-binding and product release with a change in MT-binding affinity of MTBD.[67–69] To properly model the pre-powerstroke state starting from the post-powerstroke structure (with high affinity for MT), we need to incorporate the change from α registry (with high affinity for MT) to $+\beta$ registry (with low affinity for MT) of the coiled coil stalk.[69,70] To this end, we have used iENM to computationally induce a sliding of the CC1 helix (residues 2989–3028) by four residues or half heptad relative to the CC2 helix (residues 3289–3330) toward stalk tip,[69,70] and then allow the rest of dynein to relax to a minimal-energy conformation. Accompanying the sliding of CC1 helix, we find a ∼10 ° leftward tilting of stalk relative to the head (see Fig. 2(a)). The predicted tilting of stalk, as induced by the sliding of coiled coil stalk,[69] agrees with or offers structural insights to the following findings by earlier studies:

1. The tilting and kinking of stalk were observed between the two independent molecules of the X-ray structure of *D. discoideum* dynein.[33]

2. As found by an early EM study,[16] when emerging from the dynein ring, the stalk is slightly tilted and bent to the left in the ADP-Vi-bound state, and it is slightly tilted to the right in the apo state (see Fig. 4 of Ref. 16).
3. A recent EM study observed a small tilting of stalk (in right view by 16° and in top view by 2°) relative to the head from apo state to ADP-Vi-bound state.[18] The EM-observed stalk tilting is also to the left if viewing from the same direction as in Fig. 1 (the viewing direction adopted in Fig. 5(c) of Ref. 18 is opposite to the one we use here).
4. Another EM study observed slightly different stalk angles (relative to MT) between ADP-Vi-bound state (∼58.6°) and apo state (∼54°),[71] which may be coupled to a slight tilting of stalk relative to the head.
5. According to a previous EM study,[72] the dynein ring lies within a plane parallel to the MT axis with AAA2 facing the plus end of MT (see Fig. 1(e)). Therefore, the leftward tilting of stalk is coupled to the movement of MT toward the plus end relative to dynein head (i.e., the movement of dynein toward the minus end of MT), which can be induced by a forward pulling force (toward the minus end of MT) acting on dynein head. Consequently, the tilting of stalk allows a decrease/increase in MT-binding affinity to be induced by a forward/backward pulling force, which was indeed found in a single-molecule study.[73]

Taken together, a ∼42° rotation of linker and a ∼10° tilting of stalk result in a change of ∼32° to the angle between stalk and linker (see Fig. 2(a)), which is in reasonable agreement with the EM observation of a change of the angle between tail and stalk by 24° (from 160° to 136°) between apo and ADP-Vi-bound states.[16]

The open-to-closed conformational change of AAA1–AAA2 interface (see Fig. 2(b)) involves motions within AAA1 (for example, movements of the Walker A and Walker B motifs of AAA1) and motions of AAA2 relative to AAA1 (for example, movement of the Arginine finger of AAA2).[26] What is the relative importance of intra- vs. inter-AAA motions in triggering large conformational changes in dynein ring? To answer this question, we have used iENM to induce the intra-AAA motions within the large domain of AAA1 (toward AAA3 conformation of 3qmz).[34] As a result, only a small (∼5°) swing of linker domain is induced (see Fig. S1a of the supplementary material[76]). Therefore, the inter-AAA motions between the large domains of AAA1 and AAA2 are essential to drive a large swing of linker domain, which may require the alignment of ATP-binding motifs from AAA2 (such as Arginine finger) with ATP at the primary ATPase site.[26] Indeed, a mutational study supported the importance of Arginine finger to ATP hydrolysis.[26] Another mutational study found that the recovery stroke is abolished in a Walker A mutant (K1975T) but not in a Walker B mutant (E2022Q), suggesting that the recovery stroke requires ATP binding but not hydrolysis.[10] Additionally, a FRET study showed that the tail domain remains in a post-powerstroke position in the presence of non-hydrolyzable ATP analog.[10] Therefore, the recovery stroke of dynein is coupled to an isomerization between two ATP states[10] rather than ATP binding or hydrolysis. This isomerization requires the presence of ATP and participation of ATP-binding motifs from both AAA1 (such as Walker A motif) and AAA2 (such as Arginine finger).

Transition pathway modeling reveals a sequence of structural events that couple MT binding, powerstroke, and product release

To dissect the structural basis of dynein's force generation, it is critical to probe the conformational transition from the pre-powerstroke (APP-Pi-bound) state to the post-powerstroke (apo) state. To this end, we have employed the iENM protocol (see Methods) to generate a transition pathway (consisting of a series of intermediate conformations, see Movie S1 in the supplementary material[76]) from the pre-powerstroke conformation to the post-powerstroke conformation. By analyzing the transition pathway using the reaction coordinates (see Methods section), we aim to determine the motional order of the following key parts of dynein motor domain (see Fig. 1(e)):

1. *Linker domain:* its large swing is directly responsible for force generation (powerstroke);[16]
2. *Coiled coil stalk:* the sliding between helix CC1 and CC2 is coupled to a change from weak to strong MT-binding affinity;[67–69]
3. *AAA1–AAA2:* the opening of AAA1–AAA2 interface is associated with product (ADP) release from the primary ATPase site;
4. *AAA3–AAA4, AAA4–AAA5, and AAA5–AAA6:* these relative motions between adjacent AAA+ modules may be involved in the allosteric communication from stalk to the primary ATPase site, which enables MT binding to trigger product release. For example, the AAA3–AAA4 motion may be involved in a possible signaling path: stalk → AAA4 → AAA3 → AAA2 → AAA1, while the AAA5–AAA6 motion may be involved in another possible signaling path: stalk → AAA4 → AAA5 → AAA6 → AAA1.

Many alternative pathway modeling methods have been developed to generate an energetically feasible pathway between two given protein structures based on the interpolation of certain structural properties (such as atomic coordinates, residue–residue distances etc). The use of interpolation tends to produce highly synchronized motions involving all protein residues. Instead of using structure-based interpolation, our iENM method searches for saddle points of a double-well potential function (see Methods section), and it is able to predict sequential motions of various protein parts that may shed lights on the dynamic mechanism of signaling.[54]

Indeed, our transition pathway modeling has uncovered a clear sequence of structural events in the following order (see Fig. 3 and Fig. S2 of the supplementary material[76]): stalk → AAA4–AAA5 → AAA3–AAA4 and linker → AAA1–AAA2 → AAA5–AAA6. This sequence suggests that the signaling from stalk to the primary ATPase site is mediated by the AAA3–AAA4 motion rather than the AAA5–AAA6 motion. Therefore, our finding is consistent with the

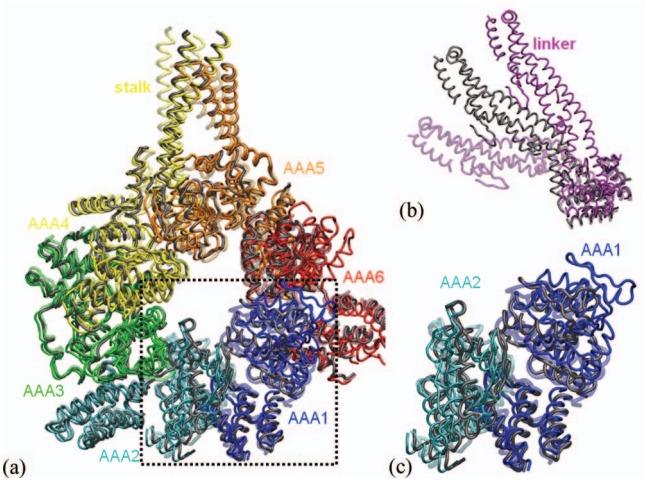

FIG. 3. Modeling of the transition from the pre-powerstroke to the post-powerstroke conformation of dynein motor domain: Panel (a) shows an intermediate conformation of the predicted transition pathway aligned with the pre-powerstroke and post-powerstroke conformations; the intermediate conformation is colored gray, the post-powerstroke conformation is opaque, and the pre-powerstroke conformation is transparent; the linker domain is removed for clarity; one can see that the intermediate conformation and pre-powerstroke conformation are similar in AAA1, AAA2, AAA5, and AAA6, while the intermediate conformation and post-powerstroke conformation are similar in stalk and buttress. Panel (b) shows the linker domain in the intermediate conformation (gray), post-powerstroke conformation (opaque), and pre-powerstroke conformation (transparent). Panel (c) shows the AAA1–AAA2 interface in the intermediate conformation (gray), post-powerstroke conformation (opaque), and pre-powerstroke conformation (transparent). The same color scheme as Fig. 1(d) is used for AAA1–AAA6 and linker.

following signaling path: stalk → AAA4 → AAA3 → AAA2 → AAA1,[16,74,75] instead of an alternative path: stalk → AAA4 → AAA5 → AAA6 → AAA1.

As shown by the predicted transition pathway, the linker domain swings in the clockwise direction over the dynein ring, forming transient contacts with residues from AAA2 to AAA5 (see Movie S2 in the supplementary material[76]). Interestingly, the truncation of linker residues 1390–1416, which form transient contacts with dynein ring during the powerstroke, was found to abolish dynein motility.[2] Therefore, these linker–ring interactions may be important in modulating the transition from pre- to post-powerstroke conformation by stabilizing or destabilizing transition intermediates. Future mutational studies will help to further probe these key interactions.

Our modeling predicts the existence of a structural intermediate with the α-registry of coiled coil stalk (corresponding to strong MT-binding affinity), closed AAA1–AAA2 interface (compatible with ADP binding, see Fig. 3(c)) and an intermediate linker orientation (between pre- and post-powerstroke position) (see Fig. 3(b)). This is akin to an ADP state in myosin V with high affinity for both F-actin and ADP (see Ref. 61).

AAA3–AAA4 closing is critical to mechano-chemical coupling of dynein

Our transition pathway modeling supports a signaling path from stalk to AAA1 via AAA3 and AAA4. Indeed, previous studies also supported the importance of nucleotide binding at AAA3–AAA4 interface to dynein function (27–29). To probe the functional role of AAA3 and AAA4, we have modeled how the absence of nucleotide binding at AAA3–AAA4 interface affects the recovery stroke. To this end, we start from the yeast dynein structure (PDB code: 3qmz), and computationally induce the opening of AAA3–AAA4 (toward the AAA1–AAA2 conformation of 3qmz) by using iENM. Then, we have repeated the modeling of pre-powerstroke conformation starting from the post-powerstroke model with open AAA3–AAA4 (by inducing the closing of AAA1–AAA2 interface, see above). The new pre-powerstroke model shows a small ($\sim 3^\circ$) swing relative to the post-powerstroke conformation (see Fig. S1b of the supplementary material[76]), suggesting that the coupling between AAA1–AAA2 closing and linker swing is greatly reduced. Therefore, the closing of AAA3–AAA4 interface by nucleotide binding is required to facilitate the ATP-driven recovery stroke of dynein. Our finding is in good agreement with a previous FRET study,[10] which found that a Walker A mutation (K2675T) in AAA3 caused large changes in FRET efficiencies, indicating a much reduced displacement of tail domain during the kinetic cycle.

CONCLUSION

In conclusion, we have used the newly solved X-ray structures of dynein motor domain[33,34] to perform a coarse-grained modeling of dynein's post- and pre-powerstroke conformation and the conformational transition between them. Our findings are summarized as follows: First, we have used NMA to identify a single normal mode that captures the coupled motions of AAA1–AAA2 closing and linker domain rotation, which allows dynein's recovery stroke to be triggered by ATP binding and isomerization.[10] Second, based on the post-powerstroke conformation solved crystallographically,[34] we have modeled dynein's pre-powerstroke conformation (with ATP or ADP-Pi bound and low MT-binding affinity) by computationally inducing AAA1–AAA2 closing and sliding of coiled coil stalk,[67–69] and the resulting model features a linker domain near the pre-powerstroke position and a slightly tilted stalk. Third, we have modeled the conformational transition from pre- to post-powerstroke conformation, which predicts a clear sequence of structural events that couple MT binding, powerstroke, and product release, and supports a signaling path from stalk to AAA1 via AAA3 and AAA4. Finally, we have found that a closed AAA3–AAA4 interface (compatible with nucleotide binding) is essential to the mechano-chemical coupling in dynein.

Our modeling offers unprecedented structural insights to the motor function of dynein as described by past single-molecule,[2,73] FRET (Ref. 10) and EM (Refs. 16, 18, and 71) studies. Our modeling also provides new predictions for future experiments, including a predicted structural intermediate with strong MT-binding affinity, closed primary ATPase site, and an intermediate linker orientation (between pre- and post-powerstroke position), and the prediction of key interactions between linker and ring that modulates the powerstroke transition.

ACKNOWLEDGMENTS

I thank funding support from American Heart Association (Grant No. 0835292N) and the National Science Foundation (Grant No. 0952736).

[1]T. Shima, K. Imamula, T. Kon, R. Ohkura, and K. Sutoh, J. Struct. Biol. **156**, 182 (2006).
[2]S. L. Reck-Peterson, A. Yildiz, A. P. Carter, A. Gennerich, N. Zhang, and R. D. Vale, Cell **126**, 335 (2006).
[3]I. R. Gibbons and A. J. Rowe, Science **149**, 424 (1965).
[4]S. Karki and E. L. Holzbaur, Curr. Opin. Cell. Biol. **11**, 45 (1999).
[5]L. M. DiBella and S. M. King, Int. Rev. Cytol. **210**, 227 (2001).
[6]R. D. Vale, Cell **112**, 467 (2003).
[7]R. B. Vallee, J. C. Williams, D. Varma, and L. E. Barnhart, J. Neurobiol. **58**, 189 (2004).
[8]K. A. Johnson, Annu. Rev. Biophys. Biophys. Chem. **14**, 161 (1985).
[9]K. Imamula, T. Kon, R. Ohkura, and K. Sutoh, Proc. Natl. Acad. Sci. U.S.A. **104**, 16134 (2007).
[10]T. Kon, T. Mogami, R. Ohkura, M. Nishiura, and K. Sutoh, Nat. Struct. Mol. Biol. **12**, 513 (2005).
[11]E. L. Holzbaur and K. A. Johnson, Biochemistry **28**, 7010 (1989).
[12]E. L. Holzbaur and K. A. Johnson, Biochemistry **28**, 5577 (1989).
[13]T. Mogami, T. Kon, K. Ito, and K. Sutoh, J. Biol. Chem. **282**, 21639 (2007).
[14]A. Habura, I. Tikhonenko, R. L. Chisholm, and M. P. Koonce, J. Biol. Chem. **274**, 15447 (1999).
[15]S. H. Tynan, M. A. Gee, and R. B. Vallee, J. Biol. Chem. **275**, 32769 (2000).
[16]S. A. Burgess, M. L. Walker, H. Sakakibara, P. J. Knight, and K. Oiwa, Nature (London) **421**, 715 (2003).
[17]N. Numata, T. Kon, T. Shima, K. Imamula, T. Mogami, R. Ohkura, and K. Sutoh, Biochem. Soc. Trans. **36**, 131 (2008).
[18]A. J. Roberts, N. Numata, M. L. Walker, Y. S. Kato, B. Malkova, T. Kon, R. Ohkura, F. Arisaka, P. J. Knight, K. Sutoh, and S. A. Burgess, Cell **136**, 485 (2009).
[19]I. R. Gibbons, B. H. Gibbons, G. Mocz, and D. J. Asai, Nature (London) **352**, 640 (1991).
[20]K. Ogawa, Nature (London) **352**, 643 (1991).
[21]M. Samso, M. Radermacher, J. Frank, and M. P. Koonce, J. Mol. Biol. **276**, 927 (1998).
[22]A. F. Neuwald, L. Aravind, J. L. Spouge, and E. V. Koonin, Genome Res. **9**, 27 (1999).
[23]M. A. Gee, J. E. Heuser, and R. B. Vallee, Nature (London) **390**, 636 (1997).
[24]M. Nishiura, T. Kon, K. Shiroguchi, R. Ohkura, T. Shima, Y. Y. Toyoshima, and K. Sutoh, J. Biol. Chem. **279**, 22799 (2004).
[25]G. Mocz and I. R. Gibbons, Biochemistry **35**, 9204 (1996).
[26]Y. Takahashi, M. Edamatsu, and Y. Y. Toyoshima, Proc. Natl. Acad. Sci. U.S.A. **101**, 12865 (2004).
[27]T. Kon, M. Nishiura, R. Ohkura, Y. Y. Toyoshima, and K. Sutoh, Biochemistry **43**, 11266 (2004).
[28]A. Silvanovich, M. G. Li, M. Serr, S. Mische, and T. S. Hays, Mol. Biol. Cell **14**, 1355 (2003).
[29]S. L. Reck-Peterson and R. D. Vale, Proc. Natl. Acad. Sci. U.S.A. **101**, 14305 (2004).
[30]C. Cho, S. L. Reck-Peterson, and R. D. Vale, J. Biol. Chem. **283**, 25839 (2008).
[31]K. Shiroguchi and Y. Y. Toyoshima, Cell Motil Cytoskeleton **49**, 189 (2001).
[32]T. Shima, T. Kon, K. Imamula, R. Ohkura, and K. Sutoh, Proc. Natl. Acad. Sci. U.S.A. **103**, 17736 (2006).
[33]T. Kon, K. Sutoh, and G. Kurisu, Nat. Struct. Mol. Biol. **18**, 638 (2011).
[34]A. P. Carter, C. Cho, L. Jin, and R. D. Vale, Science **331**, 1159 (2011).
[35]V. Tozzini, Curr. Opin. Struct. Biol. **15**, 144 (2005).
[36]A. R. Atilgan, S. R. Durell, R. L. Jernigan, M. C. Demirel, O. Keskin, and I. Bahar, Biophys. J. **80**, 505 (2001).
[37]F. Tama and Y. H. Sanejouand, Protein Eng. **14**, 1 (2001).
[38]K. Hinsen, Proteins **33**, 417 (1998).
[39]M. M. Tirion, Phys. Rev. Lett. **77**, 1905 (1996).
[40]W. G. Krebs, V. Alexandrov, C. A. Wilson, N. Echols, H. Yu, and M. Gerstein, Proteins **48**, 682 (2002).
[41]I. Bahar and A. J. Rader, Curr. Opin. Struct. Biol. **15**, 586 (2005).
[42]F. Tama and C. L. Brooks, Annu. Rev. Biophys. Biomol. Struct. **35**, 115 (2006).
[43]W. Zheng and S. Doniach, Proc. Natl. Acad. Sci. U.S.A. **100**, 13253 (2003).
[44]W. Zheng and B. R. Brooks, Biophys. J. **89**, 167 (2005).
[45]W. Zheng and B. Brooks, J. Mol. Biol. **346**, 745 (2005).
[46]H. Yu, L. Ma, Y. Yang, and Q. Cui, PLOS Comput. Biol. **3**, e23 (2007).
[47]I. Navizet, R. Lavery, and R. L. Jernigan, Proteins **54**, 384 (2004).
[48]W. Zheng, B. R. Brooks, and G. Hummer, Proteins **69**, 43 (2007).
[49]M. Cecchini, A. Houdusse, and M. Karplus, PLOS Comput. Biol. **4**, e1000129 (2008).
[50]W. Zheng, B. R. Brooks, and D. Thirumalai, Proc. Natl. Acad. Sci. U.S.A. **103**, 7664 (2006).
[51]W. Zheng, Proteins **78**, 638 (2010).
[52]W. Zheng and M. Tekpinar, BMC Struct. Biol. **9**, 45 (2009).
[53]W. Zheng and D. Thirumalai, Biophys. J. **96**, 2128 (2009).
[54]M. Tekpinar and W. Zheng, Proteins **78**, 2469 (2010).
[55]F. Tama, M. Feig, J. Liu, C. L. Brooks III, and K. A. Taylor, J. Mol. Biol. **345**, 837 (2005).
[56]A. W. Serohijos, Y. Chen, F. Ding, T. C. Elston, and N. V. Dokholyan, Proc. Natl. Acad. Sci. U.S.A. **103**, 18540 (2006).
[57]D. Tsygankov, A. W. Serohijos, N. V. Dokholyan, and T. C. Elston, J. Chem. Phys. **130**, 025101 (2009).
[58]A. W. Serohijos, D. Tsygankov, S. Liu, T. C. Elston, and N. V. Dokholyan, Phys. Chem. Chem. Phys. **11**, 4840 (2009).
[59]J. Hafner and W. Zheng, J. Chem. Phys. **132**, 014111 (2010).
[60]D. Ming and M. E. Wall, Phys. Rev. Lett. **95**, 198103 (2005).
[61]W. Zheng, Proteins **79**, 2291 (2011).
[62]F. Zhu and G. Hummer, Biophys. J. **97**, 2456 (2009).
[63]W. Zheng, J. C. Liao, B. R. Brooks, and S. Doniach, Proteins **67**, 886 (2007).
[64]H. Wang and G. Oster, Nature (London) **396**, 279 (1998).
[65]S. Fischer, B. Windshugel, D. Horak, K. C. Holmes, and J. C. Smith, Proc. Natl. Acad. Sci. U.S.A. **102**, 6873 (2005).
[66]G. Li and Q. Cui, Biophys. J. **86**, 743 (2004).
[67]A. P. Carter, J. E. Garbarino, E. M. Wilson-Kubalek, W. E. Shipley, C. Cho, R. A. Milligan, R. D. Vale, and I. R. Gibbons, Science **322**, 1691 (2008).
[68]I. R. Gibbons, J. E. Garbarino, C. E. Tan, S. L. Reck-Peterson, R. D. Vale, and A. P. Carter, J. Biol. Chem. **280**, 23960 (2005).
[69]T. Kon, K. Imamula, A. J. Roberts, R. Ohkura, P. J. Knight, I. R. Gibbons, S. A. Burgess, and K. Sutoh, Nat. Struct. Mol. Biol. **16**, 325 (2009).
[70]A. P. Carter and R. D. Vale, Biochem. Cell Biol. **88**, 15 (2010).
[71]H. Ueno, T. Yasunaga, C. Shingyoji, and K. Hirose, Proc. Natl. Acad. Sci. U.S.A. **105**, 19702 (2008).
[72]N. Mizuno, A. Narita, T. Kon, K. Sutoh, and M. Kikkawa, Proc. Natl. Acad. Sci. U.S.A. **104**, 20832 (2007).
[73]A. Gennerich, A. P. Carter, S. L. Reck-Peterson, and R. D. Vale, Cell **131**, 952 (2007).
[74]R. D. Vale, J. Cell Biol. **150**, F13 (2000).
[75]P. Hook, A. Mikami, B. Shafer, B. T. Chait, S. S. Rosenfeld, and R. B. Vallee, J. Biol. Chem. **280**, 33045 (2005).
[76]See supplementary material at http://dx.doi.org/10.1063/1.4704661 for two supplemental tables, two supplemental figures, two movies, and two Ca coordinate files in PDB format.